J. Biochem. 130, 319–329 (2001)

Structural Basis of Bacterial Photosynthetic Reaction Centers[1]

Terukazu Nogi*,[2] and Kunio Miki*,†,[3]

**Department of Chemistry, Graduate School of Science, Kyoto University, Sakyo-ku, Kyoto 606-8502; and †RIKEN Harima Institute/SPring-8, Koto 1-1-1, Mikazuki-cho, Sayo-gun, Hyogo 679-5148*

Received April 23, 2001; accepted July 3, 2001

The photosynthetic reaction center (RC) is the first membrane protein whose three-dimensional structure was revealed at the atomic level by X-ray crystallograph more than fifteen years ago. Structural information about RC made a great contribution to the understanding of the reaction mechanism of the complicated membrane protein complex. High-resolution structures of RCs from three photosynthetic bacteria are now available, namely, those from two mesophilic purple non-sulfur bacteria, *Blastochloris viridis* and *Rhodobacter sphaeroides*, and that from a thermophilic purple sulfur bacterium, *Thermochromatium tepidum*. In addition, a variety of structural studies, mainly by X-ray crystallography, are still being performed to give more detailed insight into the reaction mechanism of this membrane protein. This review deals with structural studies of bacterial RC complexes, and a discussion about the electron transfer reaction between RCs and electron donors is the main focus out of several topics addressed by these structural studies. The structural data from three RCs and their electron donors provided reliable models for molecular recognition in the primary step of bacterial photosynthesis.

Key words: bacterial photosynthetic reaction center, electron transfer, membrane protein, three-dimensional structure, X-ray crystallography.

Electron transfer coupled with the uptake of protons across the membrane is a fundamental feature of bioenergetic processes such as oxidative phosphorylation and photosynthesis, and the resulting electrochemical gradient of protons is finally utilized for ATP synthesis. Key players in bioenergetics are integral membrane proteins and co-factors embedded in the membrane protein complexes, where polypeptide chains spanning across the membrane provide a scaffold for the specific arrangement of co-factors in membrane protein complexes. Hence, structural data about membrane protein complexes contributes greatly to obtaining a profound understanding of reaction mechanisms. In fact, a great deal of effort has been made to elucidate the three-dimensional structures of membrane proteins involved in bioenergetics for the sake of functional analyses. Of such structural studies, crystallographic studies of the photosynthetic reaction center (RC) provided the first successful description of the three-dimensional structure at an atomic resolution, and the methodology established in this structural work has had a strong influence on subsequent structural studies of membrane proteins. In addition, structure analyses of RC complexes remain one of the most active fields in membrane protein structural biology. This is because it is not yet clear how the RC complex regulates the electrochemical properties of co-factors, especially that of the bacteriochlorophyll dimer (the special pair) that acts as the initiator of photosynthetic electron transfer, how the RC complex takes up protons to reduce quinone, which acts as the final electron acceptor in the complex, and how the RC complex accepts electrons from the electron carrier protein to reduce the photo-oxidized special-pair. Consequently, structure analyses of some modified RC complexes, such as mutants or complexes with substrate analogues, have been carried out extensively so as to relate structural information to physical and chemical properties, in spite of the fact that the three-dimensional structure of the native RC complex has already been determined precisely. As a result, abundant structural data have been accumulated, which can explain the functional properties of RC to some extent. Since membrane proteins involved in bioenergetics share some functional features as mentioned above, knowledge deduced from structural studies of RC complexes can provide useful information for analyses of the other membrane proteins, for example, with respect to intra- and intermolecular electron transfer and proton uptake through the

[1] This work was supported in part by the "Research for the Future" Program (JSPS-RFTF 97L00501) from the Japan Society for the Promotion of Science to KM.

[2] Present address: Photon Factory, Institute of Materials Structure Science, High Energy Accelerator Research Organization (KEK), Oho1-1, Tsukuba, Ibaraki 305-0801.

[3] To whom correspondence should be addressed: at Department of Chemistry, Graduate School of Science, Kyoto University, Sakyo-ku, Kyoto 606-8502. Phone: +81-75-753-4029, Fax: +81-75-753-4032, E-mail: miki@kuchem.kyoto-u.ac.jp

Abbreviations: BCh_A and BCh_B, bacteriochlorophyll monomers in branches A and B, respectively; *Blc., Blastochloris*; BPh_A and BPh_B, bacteriopheophytins in branches A and B, respectively;Cyt, cytochrome; D_A and D_B, bacteriochlorophylls in the special-pair in branches A and B, respectively; HiPIP, high-potential iron-sulfur protein; HM202L (an example), a mutant in which histidine at position 202 of the M subunit of RC is replaced by leucine; LHI and IHII, light-harvesting antenna proteins I and II, respectively; PSI and PSII, photosystems I and II, respectively; Q_A and Q_B, quinones in branches A and B, respectively; *Rba., Rhodobacter*; RC, reaction center; *Tch., Thermochromatium.*

membrane. This review summarizes what has been and will be shown about the three-dimensional structures of RC complexes.

Photosynthesis in bacteria

Photosynthesis is a reaction in which light energy is converted into chemical energy. The primary process of photosynthesis is carried out by a pigment-protein complex embedded in the membrane, that is, RC. In photosynthetic purple bacteria, the cyclic electron transfer reaction is performed by RC and two other components: the cytochrome (Cyt) bc_1 complex, and the soluble electron carrier protein (Fig. 1). First, RC accepts light energy from antenna proteins, and promotes a light-induced charge separation across the membrane, which results in the oxidation of the special pair and the reduction of quinone to quinol. The quinol molecule then leaves RC and moves to the Cyt bc_1 complex through the quinone-pool in the membrane. Second, the Cyt bc_1 complex re-oxidizes quinol to quinone, and the released electrons are transferred to soluble electron carriers. Third, the soluble electron carriers transport the electrons to RC through the periplasmic space. Finally, the photo-oxidized special-pair is reduced by the soluble electron carriers, and RC returns to the initial state. In the course of the oxidation and reduction of quinone, a trans-membrane electrochemical gradient of protons is formed, and the energy is utilized for ATP synthesis by ATP synthase.

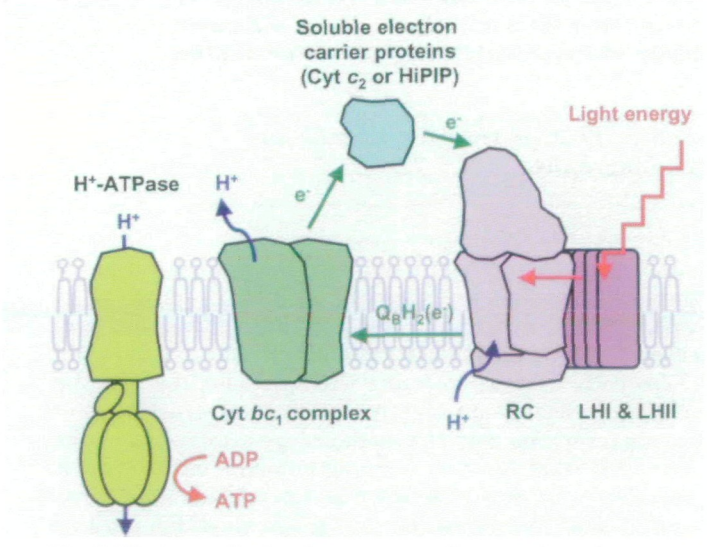

Fig. 1. **Photosynthetic electron transfer reactions in purple bacteria.** In purple bacteria, the primary reactions of photosynthesis are performed on the inner membrane, referred to as the photosynthetic membrane (shown as gray circles and lines). First, RC (pink) accepts light energy from light harvesting antenna complexes, LHI and LHII (purple). The RC complex contains various prosthetic groups that serve as the photosynthetic pigments, such as the bacteriochlrophyll dimer (special-pair), bacteriopheophytin, and quinone; charge separation occurs in this RC complex. As a result of the charge separation, quinone is reduced to quinol. Second, quinol moves to the Cyt bc_1 complex (green) through the membrane. The Cyt bc_1 complex re-oxidizes quinol to quinone, and transfers electrons to the soluble electron carrier proteins (blue). The soluble electron carrier proteins are classified into two groups, Cyt c_2 and the high-potential iron-sulfur protein (HiPIP), depending on the species used physiologically. In each case, the soluble electron carrier protein contains a redox center, such as a heme *c* group or an Fe-S cluster. Finally, the soluble electron carrier proteins move through the periplasmic space, and transfer electrons to RC. The photo-oxidized special-pair is reduced, and RC returns to the initial state. In the course of this cyclic electron transfer, the oxidation and reduction of quinone bring about a trans-membrane electrochemical gradient of protons, and the resulting energy is utilized for ATP synthesis by ATP synthase (yellow). The electron flow and proton transfer are represented by green and cyan arrows, respectively. The absorption of light energy and ATP synthesis are represented by red arrows.

The purple bacterial RC possesses bacteriopheophytin and quinone as the electron acceptor from the exited special-pair, and is, therefore, classified the same as photosystem (PS) II in plants and cyanobacteria. Significant differences are known to exist between purple bacterial RC and PSII in peripheral reactions, such as the light-harvesting mechanism and the presence of the oxygen-evolving system. However, the fundamental reactions are quite similar, for example, the charge separation initiated at the special-pair and the reduction of quinone. To date, many structural studies have been performed on purple bacterial RC complexes in order to elucidate the spatial arrangement of the prosthetic groups and the high quantum yield of the charge separation. Such studies are a help in understanding the structural features of PSII in plants and cyanobacteria.

Crystal structures of bacterial photosynthetic reaction centers

The bacterial RC is the first membrane protein whose three-dimensional structure was determined at an atomic resolution. Table I summarizes the crystallographic studies of bacterial RCs. First, the crystal structure of RC from *Blastochrolis* (*Blc.*; formerly *Rhodopseudomonas*) *viridis* was determined by the mutiple isomorphous replacement method [1PRC] (*1–3*) (Fig. 2c), and those from *Rhodobacter* (*Rba.*) *sphaeroides* were determined by the molecular replacement method [2RCR, 4RCR, 1PSS, 1PCR, and 1YST] (*4–8*) (Fig. 2d). Based on their subunit compositions, bacterial RC complexes are classified into two group (*9*): Group I is composed of three major subunits (L M, and H), and Group II possesses an additional peripheral subunit, referred to as the Cyt subunit, on the cytoplasmic side. Hence, *Rba. sphaeroides* RC and *Blc. viridis* RC belong to Group I and Group II, respectively.

In addition to these two RCs, the crystal structure of RC from *Thermochromatium* (*Tch.*; formerly *Chromatium*) *tepidum* has recently been determined at 2.2 Å resolution by the molecular replacement method [1EYS] (*10*) (Fig. 2a). *Tch. tepidum* RC possesses a Cyt subunit as in the *Blc. viridis* RC, and is therefore classified into Group II. Since the three-dimensional structure of *Tch. tepidum* RC was the first from a thermophilic organism to be determined, it is of peculiar interest to understand not only the original function of the photosynthetic apparatus, but also the thermostability of its RC molecule.

The RC complex maintains a number of prosthetic groups in the protein subunit scaffold. The prosthetic groups in the trans-membrane region apparently form two branches (A and B) that are related by a pseudo twofold axis perpendicular to the membrane plane (Fig. 2b). These two branches run from the special-pair of bacteriochlorophyll (D_A and D_B) to the non-heme iron. Each branch consists of a bacteriochlorophyll monomer (BCh_A or BCh_B),

TABLE I. **Crystallographic studies of bacterial photosynthetic reaction centers.**

Native form

PDB ID	Resolution	Space group	Organism	Classification and status	Reference
1PRC	2.30	$P4_32_12$	*Blc. viridis*	Group II	*3*
2RCR	3.10	$P2_12_12_1$	*Rba. sphaeroides*, strain R-26	Group I, Carotenoid-deficient strain	*4*
4RCR	2.80	$P2_12_12_1$	*Rba. sphaeroides*, strain R-26	Group I, Carotenoid-deficient strain	*5*
1PSS	3.00	$P2_12_12_1$	*Rba. sphaeroides*, strain 2.4.1	Group I	*6*
1PCR	2.65	$P3_121$	*Rba. sphaeroides*, strain ATCC17023	Group I, Wate chains to Q_B-site	*7*
1YST	3.00	$P2_12_12_1$	*Rba. sphaeroides*, strain Y	Group I	*8*
1EYS	2.20	$P2_12_12_1$	*Tch. tepidum*	Group II, Lipid (PE) binding	*10*

Mutant

PDB ID	Resolution	Space group	Organism	Status	Reference
1PST	3.00	$P2_12_12_1$	*Rba. sphaeroides*, strain 2.4.1	HM202L, Replacement of BChl (D_B) with BPhe	*6*
1MPS	2.55	$P3_121$	*Rba. sphaeroides*, antenna-deficient strain	FM197R/YM177F	*13*
1QOV	2.10	$P3_121$	*Rba. sphaeroides*, antenna-deficient strain	AM260W, Lipid (CL) binding	*20*
1E14	2.70	$P3_121$	*Rba. sphaeroides*, antenna-deficient strain	FM197R/GM203D	*14*
1E6D	2.30	$P3_121$	*Rba. sphaeroides*, antenna-deficient strain	FM197R/WM115F	*15*
1DXR	2.00	$P4_32_12$	*Blc. viridis*	HL168F, Terbutryn complex	*17*

Complex with Q_B-analogue, or analysis of Q_B-site

PDB ID	Resolution	Space group	Organism	Status	Reference
1AIG	2.60	$P4_32_12$	*Rba. sphaeroides*, strain R-26	Charge-separated state	*21*
1AIJ	2.20	$P4_32_12$	*Rba. sphaeroides*, strain R-26	Charge-neutral state	*21*
2PRC	2.45	$P4_32_12$	*Blc. viridis*	Ubiquinone-2 complex	*18*
3PRC	2.40	$P4_32_12$	*Blc. viridis*	Q_B-depleted state	*18*
4PRC	2.40	$P4_32_12$	*Blc. viridis*	Stigmatellin complex	*18*
5PRC	2.35	$P4_32_12$	*Blc. viridis*	Atrazine complex	*19*
6PRC	2.30	$P4_32_12$	*Blc. viridis*	DG-420314 (Triazine) complex	*19*
7PRC	2.65	$P4_32_12$	*Blc. viridis*	DG-420315 (Triazine) complex	*19*

Additional Metal binding

PDB ID	Resolution	Space group	Organism	Status	Reference
1DS8	2.50	$P4_32_12$	*Rba. sphaeroides*, strain R-26	Cd^{2+} complex, Charge-neutral state	*23*
1DV3	2.50	$P4_32_12$	*Rba. sphaeroides*, strain R-26	Cd^{2+} complex, Charge-separated state	*23*
1DV6	2.50	$P4_32_12$	*Rba. sphaeroides*, strain R-26	Zn^{2+} complex, Charge-neutral state	*23*

bacteriopheophytin (BPh_A or BPh_B), and quinone (Q_A or Q_B). A carotenoid molecule is present in the trans-membrane region near BCh_B. Branch A, mainly associated with the L subunit, is selectively utilized as the pathway of electron transfer, which is induced by charge-separation; in this process, an electron is emitted from the excited special-pair and transferred though BPh_A and Q_A. The involvement of BCh_A, which is located between the special-pair and BPh_A, in the electron transfer remains a matter of debate. Q_B is the final electron acceptor at this stage, and the reduced Q_B molecule serves as the electron carrier to the Cyt bc_1 complex.

Topics on RC structure

In addition to the structures of the three native RC complexes, the crystal structures of mutants and complexes with Q_B analogues have also been determined, and the refined models of native RC structures have been re-assessed so as to examine the biophysical and biochemical functions of RC in more detail. Since prosthetic groups play a central role in photosynthetic energy conversion, it is necessary to describe the three-dimensional arrangement of these prosthetic groups and their interactions with protein subunits precisely; this will lead to a better understanding of the functional aspects of RC. In the following sections, the most extensively discussed points about RC structures are reviewed and compared with those from the newly determined structure of *Tch. tepidum* RC.

Specific interactions with the special-pair. The crystal structures of *Rba. sphaeroides* RC have been determined by several research groups, and a number of differences have been found in the cofactor-protein interactions as compared with *Blc. viridis* RC. Especially in the coordination bonds with the Mg^{2+} ions of the special-pair, although both of the two Mg^{2+} ions in D_A and D_B in *Blc. viridis* RC are suggested to be coordinated with His residues, the presence of the coordination bonds remained in question because of the long distance between each His residue and the corresponding Mg^{2+} ion in *Rba. sphearoides* RC (*5, 11*). To test the interaction between the Mg^{2+} ion of D_B and the neighboring His residue (His M202), a mutant (HM202L) was constructed in *Rba. sphaeroides* RC and the structure of the mutant was determined [1PST] (*6*). In this mutant, the Mg^{2+} ion of D_B was depleted, which indicates that the bacteriochlorophyll of the special-pair was replaced by bacteriopheophytin. This finding strongly suggests the presence of a coordination bond in the native *Rba. sphaeroides* RC. Thereafter, the *Rba. sphaeroides* RC structure was re-determined at a higher resolution [1PCR] (*7*) using crystals with a different space group from the former crystals (*4–6, 8*). The latter structure strongly supports the existence of the coordination bond, showing that cofactor–protein interactions in the trans-membrane region are almost the same in *Blc. viridis* and *Rba. sphaeroides* RCs.

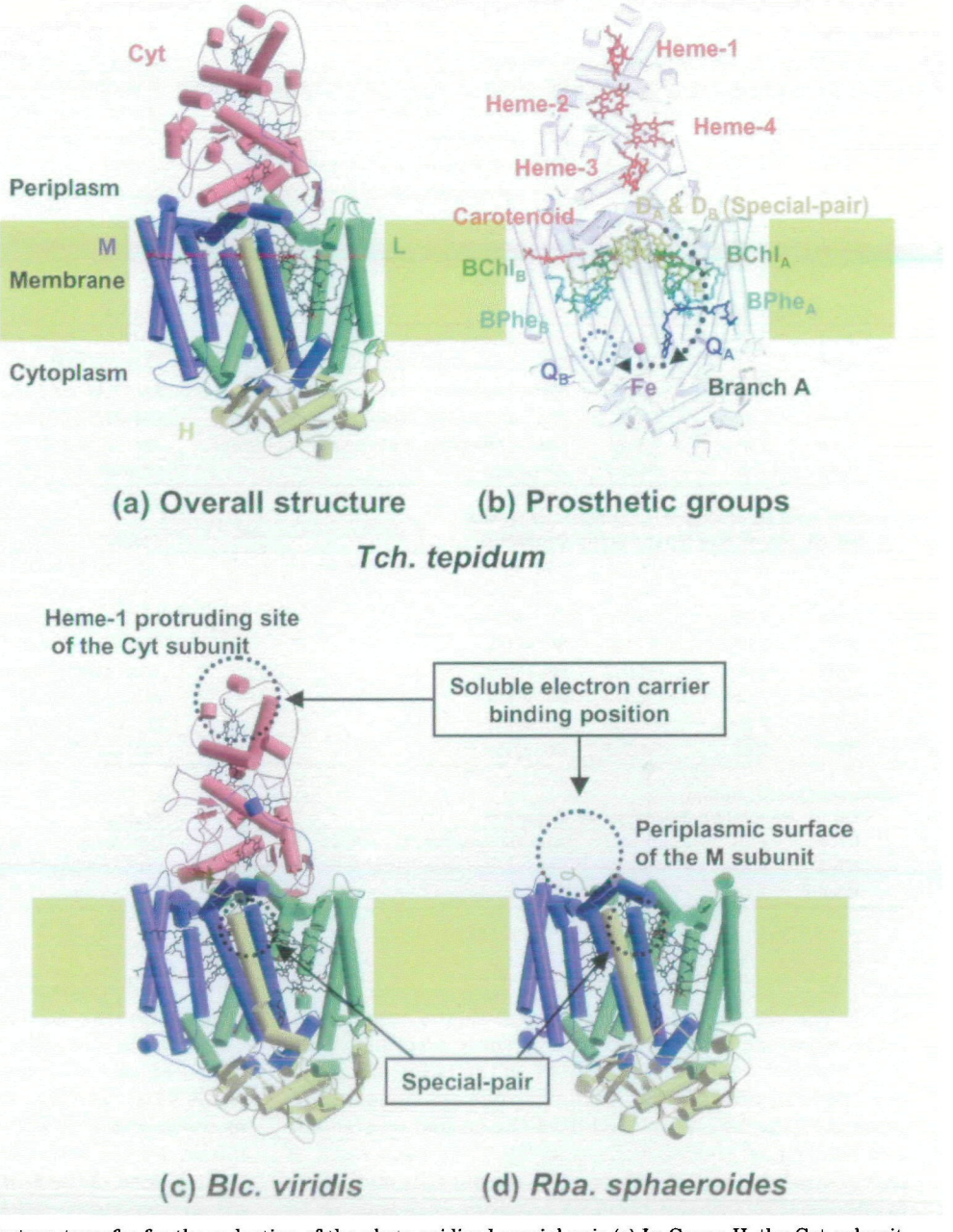

Fig. 2. **RC structures from three photosynthetic bacteria.** (a) Overall structure of *Tch. tepidum* RC: 1EYS (*10*). The polypeptide chains are colored as follows: Cyt (brown), L (green), M (purple), and H (yellow). The stick models represent the prosthetic groups embedded in the polypeptide chains. Yellow squares on both sides of the RC model represent the membrane region, and up represents the periplasmic side while down is the cytoplasmic. (b) Configuration of prosthetic groups. The stick model represents the prosthetic groups of *Tch. tepidum* RC (D_A & D_B: special-pair; BCh_A and BCh_B: bacteriochlorophyll *a* monomers; BPh_A and BPh_B: bacteriopheophytin *a* molecules; Q_A: menaquinone-8; Fe: non-heme iron; Carotenoid: spirilloxanthin; Heme-1, 2, 3, and 4: heme *c* groups). The Q_B site (blue dotted circle) is empty in this model. These prosthetic groups in the trans-membrane region apparently form two electron transfer pathways, that is, Branches A and B. However, only Branch A is utilized physiologically, and the electrons are transferred from the special-pair through BPh_A to Q_A, and consequently to Q_B. The black dotted arrows indicate electron flow among these prosthetic groups. The involvement of BCh_A in the electron transfer is still a matter of debate. (c) Overall structure of *Rba. sphaeroides* RC: 1PRC (*3*). The polypeptide chains are colored in the same manner as in (a). *Blc. viridis* RC also possesses a Cyt subunit (brown), and is, therefore, attributed to Group II. (d) Overall structure of *Rba. sphaeroides* RC: 1AIJ (*21*). Unlike the other two RCs, *Rba. sphaeroides* RC is composed of only three subunits, L (green), M (purple), and H (yellow), and is, therefore, attributed to Group I. The black dotted circles in (c) and (d) indicate the presumed positions of the soluble electron carrier proteins in the electron transfer for the reduction of the photo-oxidized special-pair. (c) In Group II, the Cyt subunit intervenes between the soluble electron carrier and the special-pair. Therefore, the Cyt subunit interacts directly with the soluble electron carrier. The binding site on the Cyt subunit is presumed to be around the heme-1 protruding site, and molecular recognition mechanisms in Group II RC are discussed in Fig. 4. (d) In Group I, the soluble electron carrier protein, Cyt c_2, transfers electrons directly to the special-pair. The binding site on the RC complex is presumed to be located on the periplasmic surface of the M subunit, which is negatively charged so as to interact with the basic surface of Cyt c_2.

In addition, these structural data indicate that the spatial arrangements of the prosthetic groups are also consistent. This is the case with *Tch. tepidum* RC, and, furthermore, the spatial arrangement of the prosthetic groups, including the four heme groups in the Cyt subunit, is quite similar to that of the former two RCs (*10*). These findings imply that the arrangement of the prosthetic groups is highly optimized in the primary reaction of photosynthesis.

The only exception concerns the hydrogen bond involving the Ring-I keto oxygen atom of D_B. In the crystal structure of *Blc. viridis* RC, this oxygen atom interacts with a Tyr residue (Tyr M195) by a hydrogen bond. In contrast, no Tyr residue is present at the same position in *Rba. sphaeroides* RC (Phe M197), and, therefore, no hydrogen bond can be formed with the oxygen atom. Since the surrounding residues would regulate the electrochemical properties of the special-pair, several mutant *Rba. sphaeroides* RCs were prepared in order to examine how the mutation affects the properties of the special-pair. Crystallographic studies of the mutant *Rba. sphaeroides* RC (FM197Y) suggested that a hydrogen bond was formed between the oxygen atom and the introduced Tyr residue. The presence of this hydrogen

bond in the mutant was also confirmed by Fourier transform infrared (FTIR) spectroscopy (*12*). In particular, the antenna-deficient strain of *Rba. sphaeroides* was employed to introduce many different single and double mutations around the Ring-I keto oxygen atom of D_B. The absence of antenna proteins made it possible to compare the properties of *in vitro* RC directly with that of *in vivo* RC. The three-dimensional structures of several of these mutants were also determined to elucidate the relationships between the observed changes in the optical and electrochemical properties and structural differences induced by these mutations [1MPS, 1E14, and 1E6D] (*13–15*). On the other hand, *Tch. tepidum* RC possesses a Tyr residue in the same position, and it is thought that a hydrogen bond is formed based on the arrangement of the Tyr residue and the special-pair. The presence of the hydrogen bond was also anticipated by FTIR. It has been proposed that this hydrogen bond could account for the increased redox potential of the special-pair and provide for the further delocalization of the positive charge in the oxidized state, as compared with those of *Rba. sphaeroides* RC (*16*).

The Ring-I keto oxygen atom of D_A interacts with the His residue by hydrogen bonding; the residue in question is His L168 in *Blc. viridis*. Mutagenesis studies of *Blc. viridis* RC indicated that the replacement of this His residue with Phe (HL168F) results in a decrease in the redox potential of the special-pair and thus an accelerated rate of charge separation. The structural change caused by this mutation was monitored by the crystal structure [1DXR] (*17*); the oxygen atom of D_A is closer to the Mg^{2+} ion of D_B due to the absence of the hydrogen bond with the His residue. Moreover, this structure was determined at the highest resolution (2.0 Å resolution) among 24 available crystal structures of bacterial RCs (Table I).

***cis*-Bond in carotenoid.** In the early stages of crystallographic studies, there was some debate about the position of the *cis*-bond in the carotenoid molecule. For example, the position of the *cis*-bond was too ambiguous to be assigned precisely in the case of *Rba. sphaeroides* RC [1PSS] (*5*). In *Blc. viridis* RC, the *cis*-bond position was formerly assigned between the 13th and 14th carbon atoms [1PRC] (*3*). However, recent crystallographic studies have provided improved electron density data, and the position was then considered to be between the 15th and 15th carbon atoms in both RCs [1YST, 2PRC, 3PRC, 4PRC, 5PRC, 6PRC, 7PRC, 1MPS, 1QOV, 1DXR, 1E14, and 1E6D] (*8, 13–15, 17–20*). In *Tch. tepidum* RC, the carotenoid is spirilloxanthin, and the electron density around the carotenoid was sufficiently clear throughout that the cis-bond could be confirmed at the same position, between 15th and 15th carbon atoms (*10*).

Reduction mechanism of Q_B. Light-induced charge separation results in the reduction of the secondary quinone, Q_B, and proton uptake from the cytoplasm, in which Q_B is reduced to a quinol, Q_BH_2, when Q_B accepts two electrons and two protons. The structures of the Q_B binding sites were not well defined in the original crystal structures. For example, the Q_B site was only about 30% occupied by ubiquinone-9 in *Blc. viridis* RC [1PRC] (*3*). In *Rba. sphaeroides* RCs, the structures of Q_B molecules varied significantly depending upon each structure determination (*4–8*). In *Tch. tepidum* RC, the occupancy was too low to construct the Q_B model at the binding pocket (*10*). Thereafter, crystallographic studies were carried out under controlled conditions. For example, the regulation of light (*21*), the reconstitution of Q_B (*18*), and the addition of herbicide, namely the Q_B analogue (*19*), were carried out so as to determine the precise configuration of Q_B at the binding pocket. In *Rba. sphaeroides* RC, X-ray diffraction data were collected under dark and luminescent conditions, which would reflect the charge-neutral [1AIJ] and the charge-separated states [1AIG], respectively (*21*). The most significant difference between these two states is the movement of the Q_B molecule (Fig. 3b). Compared with the Q_B molecule (charge-neutral state), the Q_B^- molecule (charge-separated state) moves to the cytoplasmic side, and the head group of the Q_B^- molecule twists around the isoprene tail. The binding affinity of each state of Q_B (quinone, semiquinol, and quinol) was examined in terms of its position at the binding pocket, and a quinol-releasing process was estimated. On the other hand, in *Blc. viridis* RC, the crystal structures of the Q_B-depleted state [2PRC] and the Q_B reconstituted state [3PRC] were reported (*18*). In this study, the original structure of *Blc. viridis* RC [1PRC] was also re-examined and compared with the newly determined structures, and two possible binding modes were found at the Q_B binding pocket. This was mostly consistent with the data obtained from the above-mentioned *Rba. sphaeroides* RC, in spite of the fact that the binding modes of Q_B were estimated in a slightly different way. Furthermore, the three-dimensional structures of RCs binding several herbicides were also reported [4PRC, 5PRC, 6PRC, 7PRC, and 1DXR], and the binding affinities of these herbicides were discussed (*17–19*).

Proton pathway and additional cation binding. Since the Q_B binding site is deeply buried in the cytoplasmic side of the RC complex, protons must be transferred a long distance from the cytoplasm to the Q_B binding site. Possible proton transfer pathways were identified in several structures of *Rba. sphaeroides* RC [1PCR, 1AIG, and 1AIJ] (*7, 21*), where water molecules were linked along a line from the cytoplasmic surface to the Q_B binding site (Fig. 3a). In the structure of *Tch. tepidum* RC, the most disordered regions of electron density were around the H subunit near the Q_B binding site (*10*). Hence, no distinct water chains could be defined in the region similar to that of *Rba. sphaeroides* RC.

Recently, the stoichiometric binding of cations, such as Zn^{2+} and Cd^{2+}, to the RC complex has been reported, and cation binding was found to decrease the electron transfer rate between Q_A and Q_B (*22*). The cation binding site was determined precisely by x-ray crystallography [1DS8, 1DV3, and 1DV6] (*23*), and was assigned to the entrance of the possible proton pathway on the cytoplasmic surface. The crystallographic data suggest that the bound cation inhibits proton uptake directly by capping the entrance to the pathway. It is also possible that the dynamic motions of the RC complex that accompany the proton transfer are suppressed by cation binding. In fact, Glu H173, the disordered residue in the native RC structure, was found to take a more rigid conformation in the cation-bound RC structure, which suggests a decrease in protein mobility around this region.

Lipid binding model. One lipid molecule was observed on the molecular surface of the trans-membrane region in each of the two recently determined RC structures. One is

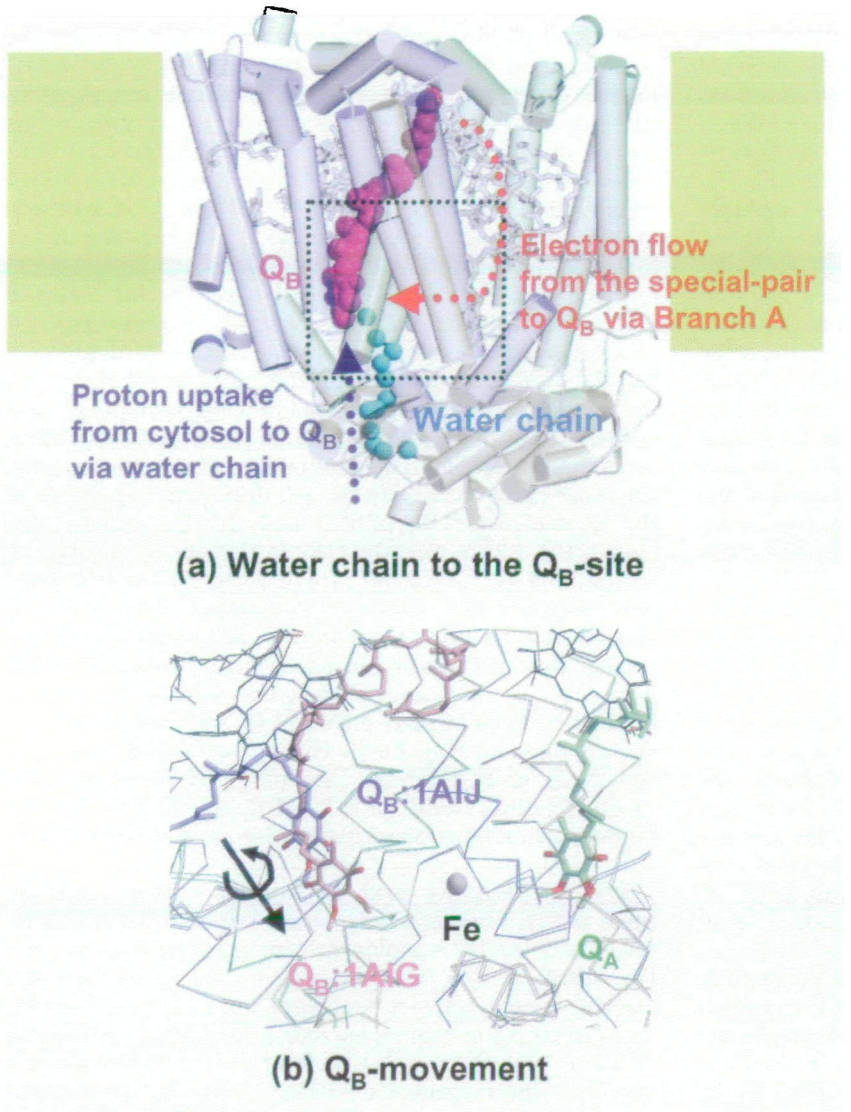

Fig. 3. **Q_B-reduction mechanism.** (a) Several water chains or clusters from cytosol to the Q_B binding site are found in the *Rba. sphaeroides* RC structures, which could serve as a proton pathway for the reduction of Q_B (blue dotted arrow). The cyan spheres represent water molecules that are linked along a line from the cytoplasmic surface to the Q_B-site; this water chain was found in the structural analysis of 1PCR (*7*). The Q_B molecule is represented by a magenta space-filling model. Similar to the diagram in Fig. 2b, electrons used for Q_B-reduction are emitted from the excited special-pair and transferred through the prosthetic groups in Branch A (red dotted arrow). Yellow squares on both sides of the RC model represent the membrane region, and up represents the periplasmic side and down the cytoplasmic side. (b) Movement of the Q_B molecule was observed in the charge separation. The area indicated by the black dotted square in (a) is highlighted in this figure. The light-purple stick model represents Q_B in the charge-neutral state, 1AIJ (*21*), and the pink model represents the charge-separated state, 1AIG (*21*). While the Q_A molecule (the green stick model) is located at almost the same position during charge separation, the Q_B molecule moves to the cytoplasmic side, and the head group twists around the isoprene tail.

caldiolipin in the mutant *Rba. sphaeroides* RC [1QOV] (*20*). The other is phosphatidylethanolamine in the native *Tch. tepidum* RC [1EYS] (*10, 24*). These lipids bind to the RC complexes with the following common features: the lipid molecule rests on the clefts of the molecular surface of RC, and these clefts are formed between the trans-membrane helix of the H subunit and the helix-bundle of the L and M subunits. The lipid molecules point their head groups towards the cytoplasm, where the phosphate group is strongly bound by electrostatic forces to relatively conserved polar residues.

Electron transfer from soluble electron carriers

In addition to the structural features of RC itself, interactions with other proteins, especially with soluble electron carrier proteins, are of interest from the viewpoint of structural analyses. In the course of photosynthetic electron transfer, RC is reduced by soluble electron carriers and then returns to the initial state. A description of the molecular recognition mechanism is important not only for understanding photosynthetic electron transfer, but also for a general understanding of intermolecular electron transfer.

Electron donors to reaction centers. In Group I RCs such as *Rba. sphaeroides* RC, soluble electron carrier proteins directly reduce the photo-oxidized special-pair, whereas in Group II RCs, such as *Blc viridis* and *Tch. tepidum* RCs, the Cyt subunit accepts electrons from soluble electron carriers and reduces the special-pair. There are four covalently bound heme groups in the Cyt subunit of most Group II RCs, which serve as the reductants of the special-pair. Recently the isolation of an RC containing only three heme groups has also been reported (*25*). The four heme groups are referred to as heme-1, heme-2, heme-4, and heme-3, proceeding from the distal side to the special-pair (Fig. 2b). Heme-1 and heme-4 are low potential, while heme-2 and heme-3 are high potential; these characteristics are conserved among all known species. For example, the redox potentials of heme-1, heme-2, heme-4, and heme-3 are –60, +320, +20, and +380 mV, respectively, in the *Blc. viridis* RC (*26*).

On the other hand, the electron donors to RC are classified as Cyt c_2, and the high-potential iron-sulfur protein (HiPIP) (*9*). In most Group I species and some Group II species, Cyt c_2 transfers electrons to RC; HiPIP is utilized as a reductant in other Group II species. HiPIP, an iron-sul-

fur protein containing a [4Fe-4S] cluster, exists abundantly in the periplasmic space of some purple bacteria. HiPIP shows 2+/3+ redox transition, and its redox potential is positive and relatively high compared to that of ferredoxins, which show a 1+/2+ redox transition (*27, 28*). In addition to HiPIP, another type of electron donor, Cyt c_8, is known to be involved in the electron transfer chain of Group II RCs (*29, 30*).

Electron transfer between RC and Cyt c_2. Due to the absence of the Cyt subunit, molecular recognition and electron transfer between RC and soluble electron carriers are relatively easy to describe in Group I RCs, in which Cyt c_2 transfers electrons directly to the special-pair of RCs. In view of the individual crystal structures of *Rba. sphaeroides* RC and *Rhodospirillum ruburum* Cyt c_2 (*31*), Cyt c_2 was assumed to dock to the acidic surface of RC on the periplasmic side by using the basic surface around the protruding part of the Cyt c_2 heme group. The binding site for Cyt c_2 was estimated to be located directly above the special-pair. Furthermore, RC and Cyt c_2 were co-crystallized to examine the interactions in the complex (*32*). Although the arrangement of Cyt c_2 to RC could not be determined precisely on the electron density map due to the low occupancy of Cyt c_2, a plausible binding model was proposed with the aid of information about their individual structures. The crystallographic study of the complex suggested that Cyt c_2 is not located at a position directly above the special-pair, but that the binding site is somewhat shifted to the M subunit side, which coincides with the results obtained from linear dichroism measurements (*33, 34*).

In contrast, the binding site in Group II RCs has been far more difficult to describe, since the Cyt subunit intervenes between the soluble electron carrier and the special-pair. It is natural to expect that all four of the heme groups in the Cyt subunit are involved in the electron transfer reaction. One would also assume that the most distal heme to the special-pair, heme-1, is the first electron acceptor. However, the midpoint redox potential of heme-1 is much lower than that of the soluble electron carrier, and heme-1 is unfavorable for accepting electrons in terms of thermodynamics. Therefore, the identity of the first electron acceptor among the four heme groups has been a matter of debate.

Since *Blc. viridis* RC was the only Group II RC whose three-dimensional structure was available, kinetic studies on electron transfer in Group II were carried out mainly using this RC. Moreover, the crystal structure of *Blc. viridis* Cyt c_2 has been determined (*35*), which provided information useful for kinetic analyses. Similar to the molecular recognition mechanism in Group I, *Blc. viridis* Cyt c_2 possesses a large basic surface around the protruding part of the heme group, and the binding site on the Cyt subunit is, therefore, expected to be negatively charged. In fact, the Cyt subunit of *Blc. viridis* RC possesses a large acidic surface around heme-1, but it remains unclear whether heme-1 is the first electron acceptor, due to its unfavorable redox potential. Recently, extensive site-directed mutagenesis studies were designed based on the structural data, and the electron transfer rate was measured in each mutant RC (*36, 37*). In the mutagenesis studies, substitutions of acidic residues near heme-1 to basic residues brought about a strong inhibition of electron transfer. These studies support the notion that the binding site for the soluble electron carrier is located near heme-1. The candidates for the first electron acceptor have thus been narrowed down to heme-1 and heme-2, since an acidic residue cluster is also proximal to heme-2.

Electron transfer between RC and HiPIP. Much less is known about electron transfer from HiPIP than from Cyt c_2. Although the three-dimensional structures of HiPIPs from several species are available and the common features of HiPIP structures have been clarified to some extent, there are no three-dimensional structures of RCs that utilize HiPIP as a reductant. The individual crystal structures of RC and HiPIP from *Tch. tepidum*, which are physiological electron transfer partners, have recently been determined (*10*). These structures are expected to pave the way for the elucidation of molecular recognition between RC and HiPIP.

As is common among the previously determined HiPIP structures, *Tch. tepidum* HiPIP possesses a large hydrophobic patch on the molecular surface near the redox center, the [4Fe-4S] cluster. Crystallographic and spectroscopic studies have shown the possibility that HiPIP molecules in solution aggregate to the dimeric state (*38–40*). However, the intermolecular interactions in the dimeric structure are not so rigid, nor so specific, and at least two kinds of dimeric interactions might be present. In both of the two dimeric states, the HiPIP monomers interact with each other through their hydrophobic surfaces, and a self-exchange of electrons has been observed between monomers. These observations suggest that the HiPIP monomer could temporally interact with another protein using its hydrophobic surface; in other words, HiPIP is assumed to dock to RC by hydrophobic interactions. On the other hand, the Cyt subunit of *Tch. tepidum* RC possesses a hydrophobic surface around heme-1; the other surfaces are relatively charged. These findings suggest that HiPIP interacts with the Cyt subunit near heme-1 by hydrophobic interactions. Furthermore, several mutations have been introduced to Rubrivivax *gelatinosus* RC so as to analyze the electron transfer rate between RC and HiPIP (*37, 41*). The mutagenesis studies have shown that the hydrophobic residues around heme-1 are involved in the intermolecular interactions, where the substitution of hydrophobic residues to charged residues results in a remarkable inhibition of electron transfer.

Redox potentials of the four heme groups in the Cyt subunit. Not only electron transfer from the soluble electron carrier to heme-1, but also that from heme-2 to heme-4 is a matter of argument. Spectroscopic studies have revealed that electrons are transferred through heme-2 and heme-3, and, consequently, to the special-pair. Since heme-4 is located between these two heme groups, heme-4 is expected to be involved in the reaction. However, the redox potential of heme-4 (+20 mV) is lower than that of both heme-2 (+320 mV) and heme-3 (+380 mV; each redox potential refers to *Blc. viridis* RC). Hence, there are two possible explanations: either electrons move directly from heme-2 to heme-3, or electrons are transferred through heme-4.

The three-dimensional structure of the mutant *Blc. viridis* RC has recently been determined, where the replacement of the Arg residue around heme-3 by Lys lowers the redox potential of heme-3 to a level lower than that of heme-2 (*42*). In this mutant, electron transfer from heme-2 to heme-3 is an uphill reaction (from +320 to +270 mV), but

the rate of the reaction is not vely different from that observed in the native RC. This observation indicates that the rate-determining step of this reaction is the electron transfer from heme-2 to heme-4, that is, electrons are presumed to be transferred *via* heme-4 in a step-wise manner. Furthermore, the experimentally suggested uphill electron transfer is supported by theoretical considerations, which indicate that the proximity of the redox centers, together with thermal activation, promote electron tunneling, even in the case of an uphill reaction (*43*). Based on this theory, the electron transfer rate calculated as a step-wise reaction shows good agreement with the observed value. These results strongly support the hypothesis that heme-1 is the first electron acceptor from the soluble electron carrier protein. Electrons would be transferred first to heme-1 in the thermodynamically uphill reaction, and thereafter to heme-2. In addition, such up-hill electron transfer is not a rare case, but has been found in other systems (*43*). The thermodynamically unfavorable reaction would have some meaning in biological function, for example, the regulation of the electron transfer rate or unidirectionality.

Evolution of the Cyt subunit. Regardless of type of soluble electron carrier proteins, the binding site on the Cyt subunit is presumed to be located near heme-1 in Group II RCs. However, the charge distributions of their molecular surfaces are quite different depending on which electron transfer partner is used, namely, there is an acidic binding site for Cyt c_2 and a hydrophobic binding site for HiPIP (Fig. 4). This phenomenon may be due to the fact that the Cyt subunits have changed their molecular surfaces to fit those of their partners.

Future studies

Many high-resolution structures are now available for individual bacterial RC complexes, in which structure–function relationships have been extensively examined as mentioned above. Further investigations will also promote a comprehensive understanding of photosynthetic reactions in the field of structural biology. Such investigations will lead to discussions on the following topics, which are thought to be universally important problems in the field.

Assembly of the photosynthetic apparatus. Bacterial RCs accept light energy from light-harvesting antenna proteins, referred to as LHI and LHII. In the photosynthetic apparatus, the RC complex is surrounded by the LHI-ring. Although the crystal structures of LHII are already available (*44–46*), the three-dimensional structure of LHI has not yet been determined. The assembly of RC and these light-harvesting proteins also remains unknown. The stoichiometry and arrangement of the LHI-ring have been investigated in several electron microscopic studies, and various arrangements were observed. For example, there is a circular (*47, 48*) or rectangular (*49*) arrangement of the LHI-ring around RC and an S-shaped arrangement of the RC-LHI dimer, in which RC is surrounded by a C-shaped LHI assembly in each RC-LHI monomer (*50*). Furthermore, an additional membrane protein, PufX, has been found in the photosynthetic apparatus, and this component is thought to affect dimerization of the RC-LHI complexes (*51*). Since the assembly would be largely susceptible to dif-

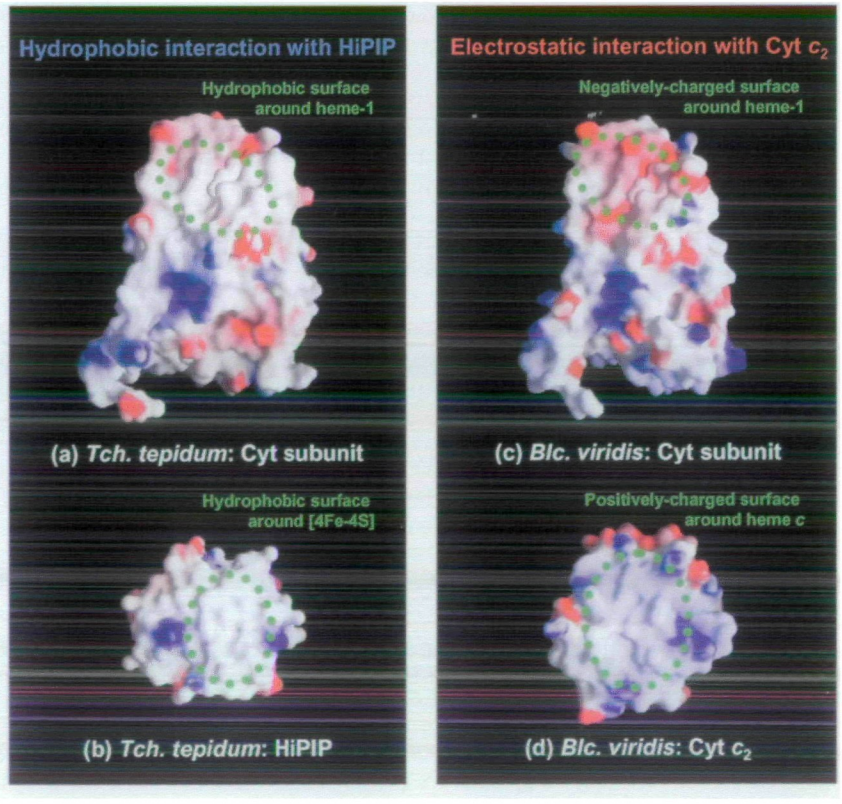

Fig. 4. **Comparison of molecular recognition mechanisms.** (a) The Cyt subunit of *Tch. tepidum* RC [1EYS] (*10*). (b) *Tch. tepidum* HiPIP [1EYT] (*10*). (c) The Cyt subunit of *Blc. viridis* RC [1PRC] (*3*). (d) *Blc. viridis* Cyt c_2 [1CO6] (*35*). The molecular surface with the charge distribution is shown in each figure. Negatively charged surfaces are colored red, and positively charged surfaces are blue. Hydrophobic or less polar surfaces are white. The binding site of each molecule is represented by a dotted green circle. (a, b) *Tch. tepidum* HiPIP possesses a large hydrophobic patch [white-colored surface indicated by the green dotted circle in (a)] on the molecular surface near the redox center, the [4Fe-4S] cluster, and this hydrophobic patch is conserved among HiPIPs of many species. On the other hand, the Cyt subunit of *Tch. tepidum* RC possesses a hydrophobic surface around the heme-1 protruding part [white-colored surface indicated by the green dotted circle in (b)]; other regions are charged. Therefore, *Tch. tepidum* HiPIP is presumed to interact with the Cyt subunit near heme-1 through hydrophobic interactions. (c, d) The heme-protruding part of *Blc. viridis* Cyt c_2 is positively charged [blue-colored surface indicated by the green dotted circle in (c)]. In contrast to the case of *Tch. tepidum* RC, the molecular surface near heme-1 of *Blc. viridis* RC is negatively charged [red-colored surface indicated by the green dotted circle in (d)], and the other regions of *Blc. viridis* RC are positively charged. Therefore, *Blc. viridis* Cyt c_2 interacts with the Cyt subunit near heme-1 through electrostatic interactions. These observations suggest that HiPIP and Cyt c_2 recognize the Cyt subunits by completely different mechanisms despite the fact that the binding sites on the two Cyt subunits are almost identical.

ferences in the preparation of the materials, observations of the intact photosynthetic apparatus are quite difficult. In order to elucidate a more detailed mechanism of energy transfer from antenna complexes to RC, it is indispensable to determine three-dimensional structures at much higher resolution under conditions that match the intact physiological state much more closely.

Structural and functional relevance to the photosystem. All of the above-mentioned bacterial RCs are derived from purple bacteria, and are thought to be the ancestors of PSII in the thylakoid membrane of higher organisms; purple bacterial RC and PSII are classified into the pheophytin-quinone type. On the other hand, RCs belonging to the iron-sulfur type are present in green sulfur bacteria and heliobacteria, and are thought to be the ancestors of PSI. The subunit composition of bacterial RC complexes is simpler than that of PSI and PSII in higher organisms. However, the basic function and assembly of bacterial RC are significantly similar to those of PSI and PSII. Three-dimensional structures of PSI and PSII have already been determined by X-ray crystallography, and the spatial arrangement of co-factors and trans-membrane helices have also been described to some extent (*52, 53*). These three-dimensional structures have shown, together with those of bacterial RCs, that RCs of any type possess common structural features. For example, a heterodimer of protein subunits forms the central part of the complex. Each monomer possesses five trans-membrane helices and maintains co-factors including the special-pair. These dimeric assemblies, including co-factors as well as protein subunits, are arranged with a pseudo twofold symmetry axis perpendicular to the membrane plane.

In the future, continuous efforts will be made to elucidate the structure–function relationship of PSI and PSII. Until the final goal is reached, however, the high-resolution structures of bacterial RCs will continue to provide important information for understanding the structural features of PSI and PSII. For example, the structure determinations of RC-herbicide complexes have explained the difference in the binding affinities of two chiral herbicides (*19*). These studies are quite helpful for understanding the effects of herbicides on the photosynthetic activities of higher plants, since the structural properties of the Q_B binding site are presumed to be similar in structure between bacterial RCs and plant photosystems.

Remarkable progress in the techniques of crystallization and structure determination has made it possible to reveal the three-dimensional structures of super-molecular complexes, including membrane proteins. In particular, progress in the crystallization method of membrane proteins should be emphasized. For example, co-crystallization with Fv-fragments (*54*), and utilization of the lipidic cubic phase (*55*) or spherical vesicles (*56*), have been developed for this purpose. Further studies in this field will make it possible to determine the structure of the super-complex of the photosynthetic apparatus more accurately, which, in turn, will lead to a profound understanding of its molecular mechanisms.

REFERENCES

1. Deisenhofer, J., Epp, O., Miki, K., Huber, R., and Michel, H. (1984) X-ray structure analysis of a membrane protein complex. Electron density map at 3 Å resolution and a model of the chromophores of the photosynthetic reaction center from *Rhodopseudomonas viridis*. *J. Mol. Biol.* **180**, 385–398
2. Deisenhofer, J., Epp, O., Miki, K., Huber, R., and Michel, H. (1985) Structure of the protein subunits in the photosynthetic reaction centre of *Rhodopseudomonas viridis* at 3Å resolution. *Nature* **318**, 618–624
3. Deisenhofer, J., Epp, O., Sinning, I., and Michel, H. (1995) Crystallographic refinement at 2.3 Å resolution and refined model of the photosynthetic reaction centre from *Rhodopseudomonas viridis*. *J. Mol. Biol.* **246**, 429–457
4. Chang, C.H., el-Kabbani, O., Tiede, D., Norris, J., and Schiffer, M. (1991) Structure of the membrane-bound protein photosynthetic reaction center from *Rhodobacter sphaeroides*. *Biochemistry* **30**, 5352–5360
5. Yeates, T.O., Komiya, H., Chirino, A., Rees, D.C., Allen, J.P., and Feher, G. (1988) Structure of the reaction center from *Rhodobacter sphaeroides* R-26 and 2.4.1: protein-cofactor (bacteriochlorophyll, bacteriopheophytin, and carotenoid) interactions. *Proc. Natl. Acad. Sci. USA* **85**, 7993–7997
6. Chirino, A.J., Lous, E.J., Huber, M., Allen, J.P., Schenck, C.C., Paddock, M.L., Feher, G., and Rees, D.C. (1994) Crystallographic analyses of site-directed mutants of the photosynthetic reaction center from *Rhodobacter sphaeroides*. *Biochemistry* **33**, 4584–4593
7. Ermler, U., Fritzsch, G., Buchanan, S.K., and Michel, H. (1994) Structure of the photosynthetic reaction centre from *Rhodobacter sphaeroides* at 2.65 Å resolution: cofactors and protein-cofactor interactions. *Structure* **2**, 925–936
8. Arnoux, B., Ducruix, A., Reiss-Husson, F., Lutz, M., Norris, J., Schiffer, M., and Chang, C.H. (1989) Structure of spheroidene in the photosynthetic reaction center from Y *Rhodobacter sphaeroides*. *FEBS Lett.* **258**, 47–50
9. Bartsch, R.G. (1991) The distribution of soluble metallo-redox proteins in purple phototrophic bacteria. *Biochim. Biophys. Acta* **1058**, 28–30
10. Nogi, T., Fathir, I., Kobayashi, M., Nozawa, T., and Miki, K. (2000) Crystal structures of photosynthetic reaction center and high-potential iron-sulfur protein from *Thermochromatium tepidum*: Thermostability and electron transfer. *Proc. Natl. Acad. Sci. USA* **97**, 13561–13566
11. el-Kabbani, O., Chang, C.H., Tiede, D., Norris, J., and Schiffer, M. (1991) Comparison of reaction centers from *Rhodobacter sphaeroides* and *Rhodopseudomonas viridis*: overall architecture and protein-pigment interactions. *Biochemistry* **30**, 5361–5369
12. Kuglstatter, A., Hellwig, P., Fritzsch, G., Wachtveitl, J., Oesterhelt, D., Mantele, W., and Michel, H. (1999) Identification of a hydrogen bond in the Phe M197→Tyr mutant reaction center of the photosynthetic purple bacterium *Rhodobacter sphaeroides* by X-ray crystallography and FTIR spectroscopy. *FEBS Lett.* **463**, 169–174
13. McAuley-Hecht, K.E., Fyfe, P.K., Ridge, J.P., Prince, S.M., Hunter, C.N., Isaacs, N.W., Cogdell, R.J., and Jones, M.R. (1998) Structural studies of wild-type and mutant reaction centers from an antenna-deficient strain of *Rhodobacter sphaeroides*: monitoring the optical properties of the complex from bacterial cell to crystal. *Biochemistry* **37**, 4740–4750
14. Fyfe, P.K., Ridge, J.P., McAuley, K.E., Cogdell, R.J., Isaacs, N.W., and Jones, M.R. (2000) Structural consequences of the replacement of glycine M203 with aspartic acid in the reaction center from *Rhodobacter sphaeroides*. *Biochemistry* **39**, 5953–5960
15. Ridge, J.P., Fyfe, P.K., McAuley, K.E., van Brederode, M.E., Robert, B., van Grondelle, R., Isaacs, N.W., Cogdell, R.J., and Jones, M.R. (2000) An examination of how structural changes can affect the rate of electron transfer in a mutated bacterial photoreaction centre. *Biochem. J.* **351**, 567–578.
16. Ivancich, A. and Mattioli, T.A. (1998) A comparative study of conserved protein interactions of the primary electron donor in photosynthetic purple bacterial reaction centers. *Photosynthesis Res.* **55**, 207–215

17. Lancaster, C.R., Bibikova, M.V., Sabatino, P., Oesterhelt, D., and Michel, H. (2000) Structural basis of the drastically increased initial electron transfer rate in the reaction center from a *Rhodopseudomonas viridis* mutant described at 2.00-Å resolution. *J. Biol. Chem.* **275**, 39364–39368
18. Lancaster, C.R. and Michel, H. (1997) The coupling of light-induced electron transfer and proton uptake as derived from crystal structures of reaction centres from *Rhodopseudomonas viridis* modified at the binding site of the secondary quinone, Q_B. *Structure* **5**, 1339–1359
19. Lancaster, C.R. and Michel, H. (1999) Refined crystal structures of reaction centres from *Rhodopseudomonas viridis* in complexes with the herbicide atrazine and two chiral atrazine derivatives also lead to a new model of the bound carotenoid. *J. Mol. Biol.* **286**, 883–898
20. McAuley, K.E., Fyfe, P.K., Ridge, J.P., Isaacs, N.W., Cogdell, R.J., and Jones, M.R. (1999) Structural details of an interaction between cardiolipin and an integral membrane protein. *Proc. Natl. Acad. Sci. USA* **96**, 14706–14711
21. Stowell, M.H., McPhillips, T.M., Rees, D.C., Soltis, S.M., Abresch, E., and Feher, G. (1997) Light-induced structural changes in photosynthetic reaction center: implications for mechanism of electron-proton transfer. *Science* **276**, 812–816
22. Utschig, L.M., Ohigashi, Y., Thurnauer, M.C., and Tiede, D.M. (1998) A new metal-binding site in photosynthetic bacterial reaction centers that modulates Q_A to Q_B electron transfer. *Biochemistry* **37**, 8278–8281
23. Axelrod, H.L., Abresch, E.C., Paddock, M.L., Okamura, M.Y., and Feher, G. (2000) Determination of the binding sites of the proton transfer inhibitors Cd^{2+} and Zn^{2+} in bacterial reaction centers. *Proc. Natl. Acad. Sci. USA* **97**, 1542–1547
24. Fathir, I., Mori, T., Nogi, T., Kobayashi, M., Miki, K., and Nozawa, T. (2001) Structure of the H subunit of the photosynthetic reaction center from the thermophilic purple sulfur bacterium, *Thermochromatium tepidum*: implications for the specific binding of the lipid molecule to the membrane protein complex. *Eur. J. Biochem.* **268**, 2652–2657
25. Masuda, S., Yoshida, M., Nagashima, K.V., Shimada, K., and Matsuura, K. (1999) A new cytochrome subunit bound to the photosynthetic reaction center in the purple bacterium, *Rhodovulum sulfidophilum*. *J. Biol. Chem.* **274**, 10795–10801
26. Dracheva, S.M., Drachev, L.A., Konstantinov, A.A., Semenov, A., Skulachev, V.P., Arutjunjan, A.M., Shuvalov, V.A., and Zaberezhnaya, S.M. (1988) Electrogenic steps in the redox reactions catalyzed by photosynthetic reaction-centre complex from *Rhodopseudomonas viridis*. *Eur. J. Biochem.* **171**, 253–264
27. De Klerk, H. and Kamen, M.D. (1966) A high-potential nonhaem iron protein from the facultative photoheterotrophe *Rhodopseudomonas gelatinosa*. *Biochim. Biophys. Acta* **112**, 175–178
28. Dus, K., De Klerk, H., Sletten, K., and Bartsch, R.G. (1967) Chemical characterization of high potential iron proteins from Chromatium and *Rhodopseudomonas gelatinosa*. *Biochim. Biophys. Acta* **140**, 291–311
29. Menin, L., Schoepp, B., Parot, P., and Vermeglio, A. (1997) Photoinduced cyclic electron transfer in *Rhodocyclus tenuis* cells: participation of HiPIP or cyt c_8 depending on the ambient redox potential. *Biochemistry* **36**, 12183–12188
30. Menin, L., Yoshida, M., Jaquinod, M., Nagashima, K.V., Matsuura, K., Parot, P., and Vermeglio, A. (1999) Dark aerobic growth conditions induce the synthesis of a high midpoint potential cytochrome c_8 in the photosynthetic bacterium *Rubrivivax gelatinosus*. *Biochemistry* **38**, 15238–15244
31. Allen, J.P., Feher, G., Yeates, T.O., Komiya, H., and Rees, D.C. (1987) Structure of the reaction center from *Rhodobacter sphaeroides* R-26: the protein subunits. *Proc. Natl. Acad. Sci. USA* **84**, 6162–6166
32. Adir, N., Axelrod, H.L., Beroza, P., Isaacson, R.A., Rongey, S.H., Okamura, M.Y., and Feher, G. (1996) Co-crystallization and characterization of the photosynthetic reaction center-cytochrome c_2 complex from *Rhodobacter sphaeroides*. *Biochemistry* **35**, 2535–2547
33. Tiede, D.M. (1987) Cytochrome *c* orientation in electron-transfer complexes with photosynthetic reaction centers of *Rhodobacter sphaeroides* and when bound to the surface of negatively charged membranes: characterization by optical linear dichroism. *Biochemistry* **26**, 397–410
34. Tiede, D.M., Vashishta, A.C., and Gunner, M.R. (1993) Electron-transfer kinetics and electrostatic properties of the *Rhodobacter sphaeroides* reaction center and soluble *c*-cytochromes. *Biochemistry* **32**, 4515–4531
35. Sogabe, S. and Miki, K. (1995) Refined crystal structure of ferrocytochrome c2 from *Rhodopseudomonas viridis* at 1.6 Å resolution. *J. Mol. Biol.* **252**, 235–247
36. Osyczka, A., Nagashima, K.V., Sogabe, S., Miki, K., Yoshida, M., Shimada, K., and Matsuura, K. (1998) Interaction site for soluble cytochromes on the tetraheme cytochrome subunit bound to the bacterial photosynthetic reaction center mapped by site-directed mutagenesis. *Biochemistry* **37**, 11732–11744
37. Osyczka, A., Nagashima, K.V., Sogabe, S., Miki, K., Shimada, K., and Matsuura, K. (1999) Comparison of the binding sites for high-potential iron-sulfur protein and cytochrome *c* on the tetraheme cytochrome subunit bound to the bacterial photosynthetic reaction center. *Biochemistry* **38**, 15779–15790
38. Couture, M.M., Auger, M., Rosell, F., Mauk, A.G., Boubour, E., Lennox, R.B., and Eltis, L.D. (1999) Investigation of the role of a surface patch in the self-association of *Chromatium vinosum* high potential iron-sulfur protein. *Biochim. Biophys. Acta* **1433**, 159–169
39. Kerfeld, C.A., Salmeen, A.E., and Yeates, T.O. (1998) Crystal structure and possible dimerization of the high-potential iron-sulfur protein from *Chromatium purpuratum*. *Biochemistry* **37**, 13911–13917
40. Parisini, E., Capozzi, F., Lubini, P., Lamzin, V., Luchinat, C., and Sheldrick, G.M. (1999) *Ab initio* solution and refinement of two high-potential iron protein structures at atomic resolution. *Acta. Cryst.* **D55**, 1773–1784
41. Osyczka, A., Nagashima, K.V., Shimada, K., and Matsuura, K. (1999) Interaction site for high-potential iron-sulfur protein on the tetraheme cytochrome subunit bound to the photosynthetic reaction center of *Rubrivivax gelatinosus*. *Biochemistry* **38**, 2861–2865
42. Chen, I.P., Mathis, P., Koepke, J., and Michel, H. (2000) Uphill electron transfer in the tetraheme cytochrome subunit of the *Rhodopseudomonas viridis* photosynthetic reaction center: evidence from site-directed mutagenesis. *Biochemistry* **39**, 3592–3602
43. Page, C.C., Moser, C.C., Chen, X., and Dutton, P.L. (1999) Natural engineering principles of electron tunnelling in biological oxidation-reduction. *Nature* **402**, 47–52
44. McDermott, G., Prince, S.M., Freer, A.A., Hawthornthwaite-Lawless, A.M., Papiz, M.Z., Cogdell, R.J., and Isaacs, N.W. (1995) Crystal structure of an integral membrane light-harvesting complex from photosynthetic bacteria. *Nature* **374**, 517–521
45. Koepke, J., Hu, X., Muenke, C., Schulten, K., and Michel, H. (1996) The crystal structure of the light-harvesting complex II (B800-850) from *Rhodospirillum molischianum*. *Structure* **4**, 581–597
46. Prince, S.M., Papiz, M.Z., Freer, A.A., McDermott, G., Hawthornthwaite-Lawless, A.M., Cogdell, R.J., and Isaacs, N.W. (1997) Apoprotein structure in the LH2 complex from *Rhodopseudomonas acidophila* strain 10050: modular assembly and protein pigment interactions. *J. Mol. Biol.* **268**, 412–423
47. Walz, T., Jamieson, S.J., Bowers, C.M., Bullough, P.A., and Hunter, C.N. (1998) Projection structures of three photosynthetic complexes from *Rhodobacter sphaeroides*: LH2 at 6 Å, LH1 and RC-LH1 at 25 Å. *J. Mol. Biol.* **282**, 833–845
48. Ikeda-Yamasaki, I., Odahara, T., Mitsuoka, K., Fujiyoshi, Y., and Murata, K. (1998) Projection map of the reaction center-light harvesting 1 complex from *Rhodopseudomonas viridis* at 10 Å resolution. *FEBS Lett.* **425**, 505–508
49. Stahlberg, H., Dubochet, J., Vogel, H., and Ghosh, R. (1998) Are

the light-harvesting I complexes from *Rhodospirillum rubrum* arranged around the reaction centre in a square geometry? *J. Mol. Biol.* **282**, 819–831
50. Jungas, C., Ranck, J.L., Rigaud, J.L., Joliot, P., and Vermeglio, A. (1999) Supramolecular organization of the photosynthetic apparatus of *Rhodobacter sphaeroides*. *EMBO J.* **18**, 534–542
51. Francia, F., Wang, J., Venturoli, G., Melandri, B.A., Barz, W.P., and Oesterhelt, D. (1999) The reaction center-LH1 antenna complex of *Rhodobacter sphaeroides* contains one PufX molecule which is involved in dimerization of this complex. *Biochemistry* **38**, 6834–6845
52. Jordan, P., Fromme, P., Witt, H.T., Klukas, O., Saenger, W., and Krauss, N., (2001) Three-dimensional structure of cyanobacterial photosystem I at 2.5 Å resolution. *Nature* **411**, 909–917
53. Zouni, A., Witt, H. T., Kern, J., Fromme, P., Krauss, N., Saenger, W., and Orth, P. (2001) Crystal structure of photosystem II from *Synechococcus elongatus* at 3.8 Å resolution. *Nature* **409**, 739–743
54. Iwata, S., Ostermeier, C., Ludwig, B., and Michel, H. (1995) Structure at 2.8 Å resolution of cytochrome *c* oxidase from *Paracoccus denitrificans*. *Nature* **376**, 660–669
55. Landau, E.M. and Rosenbusch, J.P. (1996) Lipidic cubic phases: a novel concept for the crystallization of membrane proteins. *Proc. Natl. Acad. Sci. USA* **93**, 14532–14535
56. Takeda, K., Sato, H., Hino, T., Kono, M., Fukuda, K., Sakurai, I., Okada, T., and Kouyama, T. (1998) A novel three-dimensional crystal of bacteriorhodopsin obtained by successive fusion of the vesicular assemblies. *J. Mol. Biol.* **283**, 463–474